

# A Scalable Approach to Quantum Simulation via Projection-based Embedding

Alexis Ralli,<sup>1,\*</sup> Michael I. Williams,<sup>1,†</sup> and Peter V. Coveney<sup>1,2,3,‡</sup>

<sup>1</sup>*Centre for Computational Science, Department of Chemistry,  
University College London, WC1H 0AJ, United Kingdom*

<sup>2</sup>*Advanced Research Computing Centre, University College London, WC1H 0AJ, United Kingdom*

<sup>3</sup>*Informatics Institute, University of Amsterdam, Amsterdam, 1098 XH, Netherlands*

(Dated: March 3, 2022)

Owing to the computational complexity of electronic structure algorithms running on classical digital computers, the range of molecular systems amenable to simulation remains tightly circumscribed even after many decades of work. Quantum computers hold the promise of transcending such limitations although in the current era the size and noise of these devices militates against significant progress. Here we describe a new and chemically intuitive approach that permits a subdomain of a molecule's electronic structure to be calculated accurately on a quantum device, while the rest of the molecule is described at a lower level of accuracy using density functional theory running on a classical computer. We demonstrate that our method produces improved results for molecules that cannot be simulated fully on quantum computers but which can be resolved classically at a lower level of approximation. Our algorithm is tunable, so that the size of the quantum simulation can be adjusted to run on available quantum resources. Therefore, as quantum devices become larger, our method will enable increasingly large subdomains to be studied accurately.

## I. INTRODUCTION

Quantum computing promises to enable accurate simulation of chemical systems beyond the capabilities of classical methods. Whether this aim will be achieved with so-called Noisy Intermediate-scale Quantum (NISQ) processors, is still to be seen[1–3]. While devices are improving rapidly, NISQ applications also require algorithmic tools to mitigate noise and reduce required qubit counts.

Embedding procedures work by first partitioning a system and then applying differing levels of theory to each region. An accurate but computationally expensive method is applied to a small *active region*[4, 5] The surrounding *environment* is handled with a more efficient but approximate method. This allows some of the physically relevant detail to be captured while avoiding the computational cost of accurately simulating the entire system. However, even for fairly small active regions, exact classical simulation using the Full Configuration Interaction (FCI) method quickly becomes unfeasible due to the number of Slater determinants (states) scaling factorially as  $(M)_N$ , for  $N$  electrons and  $M$  orbitals [3].

The current “gold standard” in conventional computational chemistry is coupled cluster (CC) theory, which offers a good accuracy-to-cost ratio and reduces this factorial complexity [6, 7]. The CC single double (CCSD) method scales as  $\mathcal{O}(M^6)$  [8]. The CCSD(T), which treats the triple excitations perturbatively, scales as  $\mathcal{O}(M^7)$  in time [3]. This still imposes practical limitations on system size while imperfectly approximating the effects of correlation [9]. Therefore, classical embedding methods

still inevitably inherit the shortcomings of such methods, even within a smaller active region. In short, accurately simulating quantum effects at large scale remains elusive.

Quantum computers can efficiently represent the state of general quantum systems and provide a practical way to perform quantum chemistry simulations in polynomial time [10]. However, this approach will only be possible in the fault tolerant regime, as it requires the quantum phase estimation (QPE) algorithm [11] which cannot be implemented on current NISQ quantum computers [12, 13]. Quantum algorithms designed for NISQ devices, such as the variational quantum eigensolver (VQE) [14], allow quantum systems to be studied using present day hardware; however, this is limited by the current quality and quantity of qubits. To date, the largest chemical simulation was a 12 qubit VQE study of an  $\text{H}_{12}$  chain [15].

By embedding a wave function simulation calculated on a quantum computer into a larger classical simulation, we can mitigate some of the shortfalls of classical hardware in describing quantum systems, while requiring fewer qubits and shorter quantum circuits than full-system quantum simulation. This will allow systems normally too large to study at the wave function level to be modelled via a multi-scale approach. In this way, embedding can serve as an algorithmic tool to mitigate the shortcomings of quantum and classical processors, thereby providing novel results. Additionally, as embedding methods may utilise fault-tolerant quantum simulation methods, they will continue to facilitate the study of systems larger than would otherwise be possible. Hybrid embedding methods published to date include wave function-in-DFT [16, 17], Density Matrix Embedding Theory (DMET) [18, 19] and Dynamical Mean-Field Theory [20–22] approaches.

We present a projection-based embedding method which enables the application of quantum algorithms to

\* alexis.ralli.18@ucl.ac.uk

† michael.williams.20@ucl.ac.uk

‡ p.v.coveney@ucl.ac.uk

molecules of arbitrary size while consistently improving on the results of full-system Density Functional Theory (DFT). This method outputs a Hamiltonian which can be solved using any suitable NISQ or fault-tolerant quantum algorithm, thus augmenting the usefulness of quantum processors in general. We anticipate that by targeting quantum processors at regions with strong correlation, hybrid embedding will enable novel results.

## II. PROJECTION BASED EMBEDDING

Projection-based embedding, which was first proposed by Manby *et al.* [23], provides a practical way to perform formally exact quantum embedding. We summarise the important details of their approach here.

To begin, an initial DFT calculation of the entire system is carried out using a low (cheap) level of theory. This yields a set of molecular orbitals (MOs)  $\{\psi_i | i = 1, 2, \dots, N\}$ . Each MO is formed from a linear combination of  $K$  known atomic orbital (AO) basis functions  $\{\phi_j | j = 1, 2, \dots, K\}$ :

$$|\psi_i\rangle = \sum_{j=1}^K C_{ji} |\phi_j\rangle \quad (1)$$

where  $C_{ji}$  are expansion coefficients.

Next we localize the canonical MOs  $|\psi_i\rangle$  via different localisation methods - described in further detail in the Supplementary Information. In effect, we use a unitary transform  $U$  (defined by the localization method) to spatially localize  $|\psi_i\rangle$  as much as possible. We denote these orbitals as localized molecular orbitals (LMOs):  $|\psi_i^{LMO}\rangle = U|\psi_i\rangle = \sum_{j=1}^K C_{ji}^{LMO} |\phi_j\rangle$ . In this work we localize only the occupied MOs.

Given a set of localised molecular orbitals, we partition them into two subsystems denoted *act* (active) and *env* (environment). There are different methods to do so and we summarise our approaches in the Supplementary Information. Overall we generate a set of (occupied) LMO indices  $\mathcal{K}$  and  $\mathcal{L}$  for the active and environment subsystems respectively. The resulting subsystem density matrices can then be written as:

$$\gamma^{act} = 2 \sum_{k \in \mathcal{K}} |\psi_k^{LMO}\rangle \langle \psi_k^{LMO}|, \quad (2a)$$

$$\gamma^{env} = 2 \sum_{l \in \mathcal{L}} |\psi_l^{LMO}\rangle \langle \psi_l^{LMO}|, \quad (2b)$$

for closed-shell calculations.

The total system electron density is written as a sum of subsystem densities:

$$\gamma^{total} = \gamma^{act} + \gamma^{env} = 2 \sum_{i=1}^{n_e^{total}/2} |\psi_i^{LMO}\rangle \langle \psi_i^{LMO}|. \quad (3)$$

Here each  $\gamma$  is a density matrix (defined in the AO basis). The number of electrons will also be split according to  $n_e^{total} = n_e^{act} + n_e^{env} = \text{tr}(\mathbf{S}\gamma^{act}) + \text{tr}(\mathbf{S}\gamma^{env})$ , where  $\mathbf{S}$  is the AO overlap matrix:

$$\mathbf{S}_{ij} = \langle \phi_i | \phi_j \rangle = \int d\vec{r}_1 \phi_i(1)^* \phi_j(1). \quad (4)$$

The energy of the full system can be found from its components via [24]:

$$\begin{aligned} E[\gamma^{act}, \gamma^{env}] = & \underbrace{\text{tr}(\gamma^{act} \mathbf{h}_{core}) + \mathbf{g}(\gamma^{act})}_{\text{energy of isolated act system}} + \\ & \underbrace{\text{tr}(\gamma^{env} \mathbf{h}_{core}) + \mathbf{g}(\gamma^{env})}_{\text{energy of isolated env system}} + \\ & \underbrace{\mathbf{g}(\gamma^{act}, \gamma^{env})}_{\text{nonadditive two-electron energy}}. \end{aligned} \quad (5)$$

Here  $\mathbf{h}_{core}$  is the one-electron core Hamiltonian and  $\mathbf{g}$  groups the two-electron terms - Coulomb and exchange for Hartree-Fock and exchange-correlation for DFT. The nonadditive two-electron energy is given by:

$$\mathbf{g}(\gamma^{act}, \gamma^{env}) = \mathbf{g}(\gamma^{act} + \gamma^{env}) - \mathbf{g}(\gamma^{act}) - \mathbf{g}(\gamma^{env}), \quad (6)$$

and accounts for the interaction between subsystems [24].

Next we want to solve the active system using a higher (more accurate) level of theory. The effect of the interaction between the active and environment subsystems is accounted for by additional terms in the core Hamiltonian. The Fock matrix for the active system embedded in the environment system is [23]:

$$\begin{aligned} \mathbf{F}_{emb}^{act} &= \mathbf{h}_{core} + \mathbf{V}_{emb} + \mathbf{P}_{proj}^{env} + \mathbf{g}(\gamma_{emb}^{act}) \\ &= \mathbf{h}_{emb} + \mathbf{g}(\gamma_{emb}^{act}) \end{aligned} \quad (7)$$

where:

$$\mathbf{V}_{emb} = \mathbf{g}(\gamma^{act} + \gamma^{env}) - \mathbf{g}(\gamma^{act}), \quad (8a)$$

$$\mathbf{h}_{emb} = \mathbf{h}_{core} + \mathbf{V}_{emb} + \mathbf{P}_{proj}^{env}. \quad (8b)$$

The embedding potential  $\mathbf{V}_{emb}$  describes all the interactions (nonadditive part) between the active and environment subsystems [25]. Due to the subsystem densities (Equation 3) being constructed from disjoint subsets of orthogonal orbitals, the normally difficult-to-evaluate non-additive kinetic potential (NAKP) terms [26] are exactly zero [23, 25, 27].

$\mathbf{P}_{proj}^{env}$  is a projection operator that enforces inter-subsystem (orbital) orthogonality. There are different ways to define this operator and we consider two in this work. The first definition was proposed by the Manby

and Miller groups[23]. They use a parameter ( $\mu$ ) to shift the orbital energies of the environment to high energies - effectively meaning they will never be occupied. This projector is defined as:

$$(\mathbf{P}_\mu^{\text{env}})_{ij} = \mu \langle \psi_i^{\text{LMO}} | \mathbf{P}^{\text{env}} | \psi_j^{\text{LMO}} \rangle = \mu [\mathbf{S} \gamma^{\text{env}} \mathbf{S}]_{ij}, \quad (9)$$

where  $\mu$  is some large integer,  $\mathbf{S}$  is the AO overlap matrix.  $\mathbf{P}^{\text{env}}$  is a projector defined as:

$$\mathbf{P}^{\text{env}} = \sum_{l \in \mathcal{L}} |\psi_l^{\text{LMO}}\rangle \langle \psi_l^{\text{LMO}}|. \quad (10)$$

Here we use the notation  $l \in \mathcal{L}$  to mean the sum over the set of occupied MO indices for the environment orbitals. The work in [23, 24] shows  $\mu$  is numerically robust and can usually be set to  $\mu = 10^6$ . In the limit that  $\mu \rightarrow \infty$  this method is exact. The action of this operator with the Fock matrix is:

$$(\mathbf{F} + \mathbf{P}_\mu^{\text{env}}) |\psi_k^{\text{LMO}}\rangle = \epsilon_k^{\text{act}} |\psi_k^{\text{LMO}}\rangle, \quad (11\text{a})$$

$$(\mathbf{F} + \mathbf{P}_\mu^{\text{env}}) |\psi_l^{\text{LMO}}\rangle = (\epsilon_l^{\text{env}} + \mu) |\psi_l^{\text{LMO}}\rangle \approx +\mu |\psi_l^{\text{LMO}}\rangle. \quad (11\text{b})$$

Again,  $k$  and  $l$  represent occupied LMOs of the active and environment subsystems respectively. Qualitatively the orbital energies of the active system are left unchanged and the orbitals for the environment are pushed to very high energies as  $\mu \gg \epsilon_i^{\text{env}}$  - effectively suppressing transitions to these states and stopping hybridisation.

The second approach, proposed by Kallay *et al.* [28], is to use the Huzinaga projector [29, 30]:

$$\begin{aligned} \mathbf{P}_{\text{huz}}^{\text{env}} &= -(\mathbf{F} \mathbf{P}^{\text{env}} + \mathbf{P}^{\text{env}} \mathbf{F}) \\ &= -\frac{1}{2} (\mathbf{F} \gamma^{\text{env}} \mathbf{S} + \mathbf{S} \gamma^{\text{env}} \mathbf{F}) \end{aligned} \quad (12)$$

Note that the  $-\frac{1}{2}$  prefactor is needed for closed-shell systems. This operator enforces orthogonality of the occupied orbitals of each subsystem [31]. The form of this operator increases the orbital energy for the occupied environment orbitals and leaves the active system unchanged. We write its action formally as:

$$(\mathbf{F} + \mathbf{P}_{\text{huz}}^{\text{env}}) |\psi_k^{\text{LMO}}\rangle = \epsilon_k^{\text{act}} |\psi_k^{\text{LMO}}\rangle, \quad (13\text{a})$$

$$\begin{aligned} (\mathbf{F} + \mathbf{P}_{\text{huz}}^{\text{env}}) |\psi_l^{\text{LMO}}\rangle &= (\epsilon_l^{\text{env}} - 2\epsilon_l^{\text{env}}) |\psi_l^{\text{LMO}}\rangle \\ &= -1\epsilon_l^{\text{env}} |\psi_l^{\text{LMO}}\rangle, \end{aligned} \quad (13\text{b})$$

As  $\epsilon_l^{\text{env}}$  for occupied orbitals should always be negative, this ensures the filled environment orbitals will always have a positive energy and thus will never be filled.

Whereas in Equation 11b, for the unlikely case that  $\mu < \epsilon_i^{\text{env}}$ , the environment MOs are not projected to high enough energies to stop hybridization. This scenario is highly improbable, but could still occur.

The Huzinaga formalism guarantees that  $[\mathbf{P}_{\text{huz}}^{\text{env}}, \mathbf{F}_{\text{emb}}^{\text{act}}] = 0$  and removes the need for the  $\mu$  parameter shift [32]. This methodology ensures that the environment orbitals  $|\psi_{l \in \mathcal{L}}^{\text{LMO}}\rangle$  are eigenfunctions of  $(\mathbf{F} + \mathbf{P}_{\text{huz}}^{\text{env}})$  and when solving the active system (Equation 7) the resultant canonical active orbitals will be orthogonal to them.

The energy of the active system embedded in the environment is given by:

$$\begin{aligned} E[\gamma_{\text{emb}}^{\text{act}}; \gamma^{\text{act}}, \gamma^{\text{env}}] &= \mathcal{E}[\gamma_{\text{emb}}^{\text{act}}] + E[\gamma_{\text{env}}] + \mathbf{g}(\gamma^{\text{act}}, \gamma^{\text{env}}) \\ &\quad + \text{tr}((\gamma_{\text{emb}}^{\text{act}} - \gamma^{\text{act}})(\mathbf{V}_{\text{emb}} + \mathbf{P}_{\text{proj}}^{\text{env}})) \end{aligned} \quad (14)$$

colloquially denoted as a DFT-in-DFT calculation.

We use the same notation as [24], where  $\mathcal{E}$  differs from  $E$  as it allows for different functionals to be applied and is computed from the embedded density matrix of the active system. Note that Equation 7 is solved self-consistently to give  $\gamma_{\text{emb}}^{\text{act}}$ . Equation 14 reduces to Equation 5 for the case that the active and environment regions are treated at the same level of theory [24].

Importantly  $\mathcal{E}[\gamma_{\text{emb}}^{\text{act}}] = \text{tr}(\gamma_{\text{emb}}^{\text{act}} \mathbf{h}_{\text{core}}) + \mathbf{g}(\gamma_{\text{emb}}^{\text{act}})$  and does not involve  $\mathbf{V}_{\text{emb}}$  or  $\mathbf{P}_{\text{proj}}^{\text{env}}$ . The final term in Equation 14 is a first-order correction that accounts for the difference between  $\mathbf{g}(\gamma^{\text{act}}, \gamma^{\text{env}})$  and  $\mathbf{g}(\gamma_{\text{emb}}^{\text{act}}, \gamma^{\text{env}})$ , and corrects for the fact that in general  $\gamma^{\text{act}} \neq \gamma_{\text{emb}}^{\text{act}}$  [33].

This projection based embedding approach then allows for the active system to be treated using some wave function level of theory and therefore studied using a quantum computer. The electronic energy for this is given by [24]:

$$\begin{aligned} E[\Psi_{\text{emb}}^{\text{act}}; \gamma^{\text{act}}, \gamma^{\text{env}}] &= \langle \Psi_{\text{emb}}^{\text{act}} | \mathbf{H}_{\text{emb}} | \Psi_{\text{emb}}^{\text{act}} \rangle + E[\gamma_{\text{env}}] \\ &\quad + \mathbf{g}(\gamma^{\text{act}}, \gamma^{\text{env}}) - \text{tr}(\gamma^{\text{act}}(\mathbf{V}_{\text{emb}} + \mathbf{P}_{\text{proj}}^{\text{env}})) \end{aligned} \quad (15)$$

Importantly  $\mathbf{H}_{\text{emb}} = \mathbf{h}_{\text{emb}} + \mathbf{g}(\Psi_{\text{emb}}^{\text{act}})$ , where  $\mathbf{g}(\Psi_{\text{emb}}^{\text{act}})$  is the two-electron operator for a given wave function method and  $\mathbf{h}_{\text{emb}}$  is the embedded core Hamiltonian (Equation 8b) which depends on  $\gamma^{\text{act}}$  and  $\gamma^{\text{env}}$  [34]. As the embedding terms have been included in  $\mathbf{H}_{\text{emb}}$ , the final correction term is therefore slightly different to Equation 14 [33]. The wave function calculation in Equation 15 includes contributions from  $(\mathbf{V}_{\text{emb}} + \mathbf{P}_{\text{proj}}^{\text{env}})$  - this acts like:  $\text{tr}(\gamma_{\text{emb}}^{\text{act}}(\mathbf{V}_{\text{emb}} + \mathbf{P}_{\text{proj}}^{\text{env}}))$ . The correction therefore only requires subtracting  $\text{tr}(\gamma^{\text{act}}(\mathbf{V}_{\text{emb}} + \mathbf{P}_{\text{proj}}^{\text{env}}))$ , unlike in Equation 14, where  $\mathcal{E}$  does not use  $(\mathbf{V}_{\text{emb}} + \mathbf{P}_{\text{proj}}^{\text{env}})$  to calculate the energy of the active system.

For the embedded system, truncating the virtual LMOs significantly reduces the computational cost for the embedded wave function calculation [35]. This would

reduce the quantum resources required, as each qubit represents an orbital. We leave this for future work.

### III. METHODS

We studied the performance of our wave function projection based embedding method on a selected set of molecular systems. We developed a python package, Nbed, that utilizes the PySCF and Openfermion quantum chemistry packages to build each embedded model [36, 37]. The package outputs a qubit Hamiltonian for the wave function portion of an embedded problem and the classical energy corrections from density functional theory. This is freely available for use on GitHub [38].

For all calculations presented, the minimal *STO-3G* basis set was employed. Each global DFT calculation performed, prior to orbital localisation, used the *B3LYP* functional. The Intrinsic Bonding Orbitals (IBO) or Subsystem Projected AO DEcomposition (SPADE) localisation procedures are used in order to isolate the molecular orbitals to the active and environment subsystem from pre-selected active atoms. A threshold of 95% was used to select the active region when IBO was employed. This paper’s Supplementary Information goes into further detail on each localisation strategy. We performed both the  $\mu$ -shift and Huzinaga methods for each. A Hartree-Fock calculation for the active system, using the modified core Hamiltonian, was performed for each molecular system. The second quantized molecular Hamiltonian was then constructed with Openfermion and converted to a qubit Hamiltonian using the in-built Jordan-Wigner transformation [39]. Post Hartree-Fock methods were performed with PySCF. The frozen core approximation is never used and all virtual orbitals were included in the wave function calculations. Only the occupied environment orbitals were removed from the wave function calculations of the active systems.

For the single point electronic structure calculations, each result is compared to full system CCSD(T) calculation. Each molecular geometry was obtained from PubChem [40]. The potential energy surface for OH bond stretching in water was compared to a full configuration interaction (FCI) calculation at each step, where the embedded molecular Hamiltonian at each geometry was diagonalized to find the ground state energy of the active system.

## IV. RESULTS AND DISCUSSION

### A. Molecular Ground State Energy

Results for embedding calculations of molecular ground state energies of small molecules are shown in Figure 2, with numerical values available in this paper’s Supplementary Information. The results for the same calculations using IBO localized orbitals can also be found

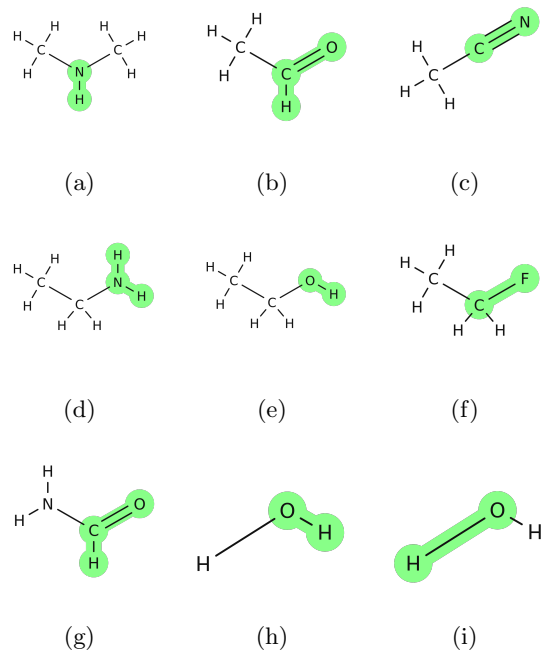


FIG. 1: Planar representations of the molecules used in embedding calculations. Atoms shaded in green were selected as active for localisation procedures. Images were generated using MolView [41].

- (a) N-methylmethanamine; (b) acetaldehyde; (c) acetonitrile; (d) ethanamine; (e) ethanol; (f) flouroethane; (g) formamide; (h) water (fixed bond active); (i) water (stretching bond active)

in the Supplementary Information. Figure 1 shows the partition of each molecule into active and environment orbitals which underlies our localisation methods.

Our results show increased accuracy in calculated molecular ground state energies. The Hamiltonians output using both localisation methods are reduced in size significantly; however, they still exceed the limit of what is practical to exactly solve using classical computers. Reported energies were calculated using CCSD(T)-in-DFT embedding to illustrate the application of this method to larger molecules than would be feasible using current quantum processors. As hardware continues to develop, implementation of our algorithm will be able to furnish novel results. Typically, results for the  $\mu$ -shift and Huzinaga projectors are very similar, however; the Huzinaga projector usually produces more accurate energies, in line with previous research [32]. The number of terms in the Jordan-Wigner encoded qubit Hamiltonian,  $|H|$ , is typically very similar between the two projection methods.

In comparing the two localisation methods, we find that for acetonitrile and formamide, SPADE and IBO partition the active system in a similar way. This results in a similar number of active MOs and hence the

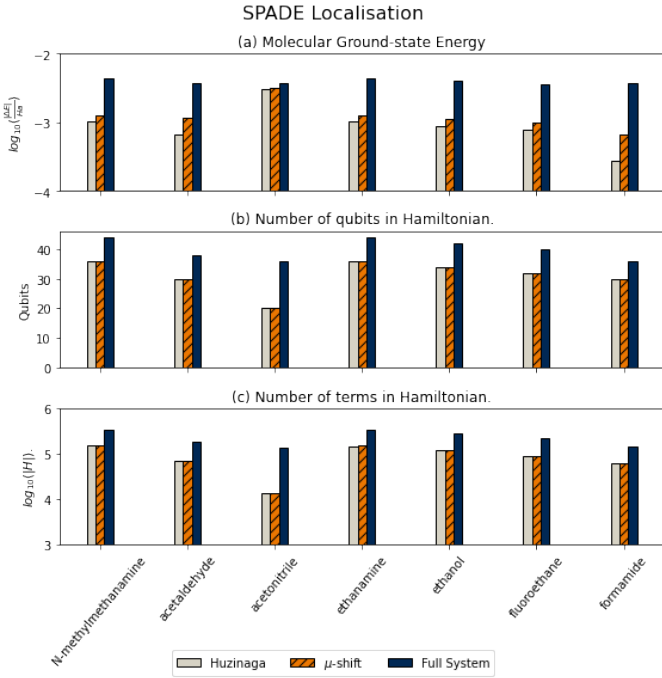


FIG. 2: Results for embedding of small molecules using the SPADE localisation method. (a) Ground state energies for small molecules, with full-system DFT energy as reference,  $\mu$ -shift CCSD embedding energy in orange and Huzinaga CCSD embedding in grey. All values are given as a difference from whole system CCSD(T) energy. (b) The number of qubits needed to describe the embedded Hamiltonian, with reference showing the number required for the full system Hamiltonian. (c) The number of terms in the Jordan-Wigner encoded qubit Hamiltonian for each molecule. Again the reference gives the number needed for the full system Hamiltonian.

ground state estimation and resource requirements are very similar for these systems. For the majority of the molecules we study, SPADE includes more MOs, resulting in significantly more accurate ground state energies while still reducing the size of the Hamiltonian. However, by reducing the threshold of assigning the localized MOs from IBO to the active region, additional MOs could be included giving a similar result. See the Supplementary Information for further details.

### B. Strong Correlation

The impact of active region selection is demonstrated by our results in Figure 3. We consider the bond dissociation of an OH bond in water - where at high bond lengths a correlated state is created. We perform projection based embedding calculations, at different molecular geometries, for two different active regions. One has the atoms in the fixed OH bond set active and the other has

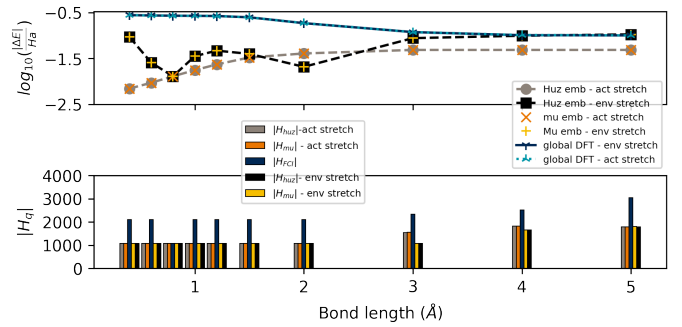


FIG. 3: Potential energy curve for H<sub>2</sub>O, with changing OH bond length. *Active stretch* result has changing OH bond as active region and *environment stretch* result has fixed OH bond selected as the active region. These results use SPADE localisation. For each data the full problem is reduced from 14 to 12 qubits, with the number of active MOs being 4, in all cases. (top) Shows the *log* base 10 error with respect to the exact FCI energy. (bottom) The number of terms in the Jordan-Wigner encoded qubit Hamiltonian obtained with each method. Numerical details are available in this paper's Supplementary Information.

the atoms in the changing OH bond set active. We show this pictorially in Fig. 1h and 1i.

At near equilibrium bond lengths, we see a similar performance between the different active systems (Figure 3). This is due to the symmetrical structure of H<sub>2</sub>O, hence at low bond lengths there is little difference between the two active regions. In fact, the third data point gives results for the scenario where both OH bonds are the same length and consequently is why the results for the different active regions are the same here. However, in the correlated regime - at large bond lengths - selecting the active region to encompass the stretched atoms leads to significant improvements in energy calculation over DFT alone. This is due to correlation being effectively captured in the wave function calculation. In contrast, the full DFT calculation is plagued by deficiencies of current approximate exchange-correlation functionals [42, 43]. We see in Figure 3 that the global DFT calculation overestimates the bond dissociation energy. This problem is attributed to static correlation [42]. As there is no systematic way to improve the exchange-correlation functionals, the way forward to describe such systems may be hybrid quantum-classical embedding. Here quantum processors could be exploited most effectively by application to only those regions of a molecule that are highly correlated.

### C. MO localisation method

For the work we have presented, we only use the SPADE and IBO localized molecular orbitals. The mo-

tivation for using SPADE is primarily that it doesn't require a parameterised heuristic to determine the active and environment subsystems. In the IBO approach, we calculate the percentage of the  $i_{th}$  LMO over atoms a user defines as the active subsystem. Any LMO that has a percentage higher than 95 % we assign to the active region. The SPADE approach doesn't require this threshold hyper-parameter. However, it does use a function of the molecular orbital coefficient matrix. Further details on both approaches are given in the Supplementary Information.

The IBOs were used as they only depend on the intrinsic atomic orbital charges, rather than Mulliken charges which change erratically depending on the basis set used [44]. IBOs are therefore always well-defined, whereas other localization methods - such as Pipek-Mezey orbitals [45], which depend on the Mulliken charges [46] - are unphysically tied to the basis set used [44].

The effect of different localisation methods for this embedding method [45, 47–49] would be an interesting area to explore. Our software package Nbed can run any method given by PySCF, and users can also build their own localisation strategies themselves.

## V. CONCLUSION

We have used the projection-based embedding technique [23] to reduce the size of an electronic structure calculation studied at the wave function level. The molecular problem is split into active and environment parts, each solved using different levels of theory. The active part is treated using a wave function approach and an embedded qubit Hamiltonian is generated. Solving this provides  $E_{act}^{WF} = \langle \Psi_{emb}^{act} | \mathbf{H}_{emb} | \Psi_{emb}^{act} \rangle$ . This is similar to the own n-layered integrated molecular orbital and molecular mechanics (ONIOM) subtractive framework [50]. The whole system and environment are treated using density functional theory and the overall electronic energy is found as  $E_{total} = E_{total}^{DFT} - E_{act}^{DFT} + E_{act}^{WF}$  [32, 34]. What is included in the active region can be modified and thus the size of the quantum problem varied. This allows users to tune their problem to available hardware.

For a small collection of molecules, too large for whole system quantum simulation and classical FCI, we have

shown that this method produces more accurate energies than full system DFT when each is compared to full system CCSD(T). Furthermore, we have shown its ability to capture the effects of strong correlation by investigating the bond dissociation of  $\text{H}_2\text{O}$ .

As this approach generates an embedded qubit Hamiltonian, it is agnostic to the quantum algorithm used to solve  $H_{emb}$ . NISQ friendly approaches such as the VQE algorithm can therefore be used, but also fault-tolerant methods such as quantum phase estimation (QPE) [10].

Moreover, as our method outputs a qubit Hamiltonian, different resource reduction techniques can be used in conjunction with it, for example, the contextual-subspace approach of Kirby *et al.* [51] or the entanglement forging approach of Eddins [52]. Similarly, the  $\mathcal{Z}_2$ -symmetries of the problem can also be removed via qubit tapering [53].

As our method does not rely on imposing constraints on the system studied or costly parameter fitting, it may be reasonably combined with other hybridisation techniques which do [16, 54].

Further work is planned to develop this method. As significant resource reduction is achieved by localisation of only the occupied orbitals, virtual orbital localisation could lead to a greater reduction in computational resources [35].

We anticipate that our code will allow researchers to study molecules of real chemical interest on quantum computers. We welcome readers to make use of this, which is freely available on Github [38].

## ACKNOWLEDGMENTS

A. R. and M. I. W. acknowledge support from the Engineering and Physical Sciences Research Council (EPSRC) (EP/L015242/1 and EP/S021582/1 respectively). P. V. C. is grateful for funding from the European Commission for VECMA (800925) and EPSRC for SEAVEA (EP/W007711/1). We would like to thank Dr. D. Kranzlmüller at the Leibniz Supercomputing Centre (LRZ), who provided access to their ATOS Quantum Learning Machine simulator for some of the computations. The authors would also like to thank Dr. David A. Herrera-Martí for useful preliminary discussions on embedding. A.R. and M.I.W. contributed equally to this work.

- 
- [1] B. A. Cordier, N. P. D. Sawaya, G. G. Guerreschi, and S. K. McWeeney, Biology and medicine in the landscape of quantum advantages (2021), arXiv:2112.00760 [quant-ph].
- [2] H.-P. Cheng, E. Deumens, J. K. Freericks, C. Li, and B. A. Sanders, Application of quantum computing to biochemical systems: A look to the future, *Frontiers in Chemistry* **8**, 10.3389/fchem.2020.587143 (2020).
- [3] S. McArdle, S. Endo, A. Aspuru-Guzik, S. C. Benjamin, and X. Yuan, Quantum computational chemistry, *Reviews of Modern Physics* **92**, 10.1103/RevModPhys.92.015003 (2020).
- [4] Q. Sun, G. Kin, and L. Chan, Quantum embedding theories, *Acc. Chem. Res.* **29**, 43 (2016).
- [5] B. Bauer, S. Bravyi, M. Motta, and G. K.-L. Chan, Quantum algorithms for quantum chemistry and quantum materials science, *Chemical Reviews* **120**, 12685 (2020), pMID: 33090772, <https://doi.org/10.1021/acs.chemrev.9b00829>.
- [6] R. J. Bartlett and M. Musial, Coupled-cluster theory in

- quantum chemistry, *Reviews of Modern Physics* **79**, 291 (2007).
- [7] J. Romero, R. Babbush, J. R. McClean, C. Hempel, P. J. Love, and A. Aspuru-Guzik, Strategies for quantum computing molecular energies using the unitary coupled cluster ansatz, *Quantum Science and Technology* **4**, 014008 (2018).
- [8] G. D. Purvis III and R. J. Bartlett, A full coupled-cluster singles and doubles model: The inclusion of disconnected triples, *Journal of Chemical Physics* **76**, 1910 (1982).
- [9] J. M. Herbert, Fantasy versus reality in fragment-based quantum chemistry, *Journal of Chemical Physics* **151**, 10.1063/1.5126216 (2019).
- [10] A. Aspuru-Guzik, A. D. Dutoi, P. J. Love, and M. Head-Gordon, Simulated quantum computation of molecular energies, *Science* **309**, 1704 (2005).
- [11] A. Y. Kitaev, Quantum measurements and the abelian stabilizer problem, *arXiv preprint quant-ph/9511026* (1995).
- [12] P. J. O’Malley, R. Babbush, I. D. Kivlichan, J. Romero, J. R. McClean, R. Barends, J. Kelly, P. Roushan, A. Tranter, N. Ding, *et al.*, Scalable quantum simulation of molecular energies, *Physical Review X* **6**, 031007 (2016).
- [13] H. Mohammadbagherpoor, Y.-H. Oh, A. Singh, X. Yu, and A. J. Rindos, Experimental challenges of implementing quantum phase estimation algorithms on ibm quantum computer, *arXiv preprint arXiv:1903.07605* (2019).
- [14] A. Peruzzo, J. McClean, P. Shadbolt, M.-H. Yung, X.-Q. Zhou, P. J. Love, A. Aspuru-Guzik, and J. L. O’Brien, A variational eigenvalue solver on a photonic quantum processor, *Nature Communications* **5**, 1 (2014).
- [15] G. A. Quantum, Collaborators\*†, F. Arute, K. Arya, R. Babbush, D. Bacon, J. C. Bardin, R. Barends, S. Boixo, M. Broughton, B. B. Buckley, *et al.*, Hartree-fock on a superconducting qubit quantum computer, *Science* **369**, 1084 (2020).
- [16] M. Rossmannek, P. K. Barkoutsos, P. J. Ollitrault, and I. Tavernelli, Quantum HF/DFT-embedding algorithms for electronic structure calculations: Scaling up to complex molecular systems, *Journal of Chemical Physics* **154**, 114105 (2021), <https://doi.org/10.1063/5.0029536>.
- [17] H. Ma, M. Govoni, and G. Galli, Quantum simulations of materials on near-term quantum computers, *npj Computational Materials* **6**, 85 (2020).
- [18] N. C. Rubin, A hybrid classical/quantum approach for large-scale studies of quantum systems with density matrix embedding theory (2016), *arXiv:1610.06910* [quant-ph].
- [19] T. Yamazaki, S. Matsuura, A. Narimani, A. Saidmurodov, and A. Zaribafyan, Towards the practical application of near-term quantum computers in quantum chemistry simulations: A problem decomposition approach (2018), *arXiv:1806.01305* [quant-ph].
- [20] B. Bauer, D. Wecker, A. J. Millis, M. B. Hastings, and M. Troyer, Hybrid quantum-classical approach to correlated materials, *Physical Review X* **6**, 031045 (2016).
- [21] J. M. Kreula, L. García-Álvarez, L. Lamata, S. R. Clark, E. Solano, and D. Jaksch, Few-qubit quantum-classical simulation of strongly correlated lattice fermions, *EPJ Quantum Technology* **3**, 11 (2016).
- [22] T. Steckmann, T. Keen, A. F. Kemper, E. F. Dumitrescu, and Y. Wang, Simulating the Mott transition on a noisy digital quantum computer via Cartan-based fast-forwarding circuits (2021), *arXiv:2112.05688* [quant-ph].
- [23] F. R. Manby, M. Stella, J. D. Goodpaster, and T. F. Miller, A simple, exact density-functional-theory embedding scheme, *Journal of Chemical Theory and Computation* **8**, 2564 (2012), pMID: 22904692.
- [24] D. Claudino and N. J. Mayhall, Automatic partition of orbital spaces based on singular value decomposition in the context of embedding theories, *Journal of Chemical Theory and Computation* **10**.1021/acs.jctc.8b01112 (2019).
- [25] S. J. R. Lee, M. Welborn, F. R. Manby, and T. F. Miller, Projection-based wavefunction-in-DFT embedding, *Accounts of Chemical Research* **52**, 1359 (2019).
- [26] O. Roncero, M. de Lara-Castells, P. Villarreal, F. Flores, J. Ortega, M. Paniagua, and A. Aguado, An inversion technique for the calculation of embedding potentials, *Journal of Chemical Physics* **129**, 184104 (2008).
- [27] T. A. Barnes, J. D. Goodpaster, F. R. Manby, and T. F. Miller III, Accurate basis set truncation for wavefunction embedding, *Journal of Chemical Physics* **139**, 024103 (2013).
- [28] B. Hégely, P. R. Nagy, G. G. Ferenczy, and M. Kállay, Exact density functional and wave function embedding schemes based on orbital localization, *Journal of Chemical Physics* **145**, 064107 (2016).
- [29] S. Huzinaga and A. A. Cantu, Theory of separability of many-electron systems, *Journal of Chemical Physics* **55**, 5543 (1971).
- [30] E. Francisco, A. Martín Pendás, and W. Adams, Generalized huzinaga building-block equations for nonorthogonal electronic groups: Relation to the Adams–Gilbert theory, *Journal of chemical physics* **97**, 6504 (1992).
- [31] T. Shimazaki, K. Kitaura, D. G. Fedorov, and T. Nakajima, Group molecular orbital approach to solve the huzinaga subsystem self-consistent-field equations, *Journal of Chemical Physics* **146**, 10.1063/1.4976646 (2017).
- [32] D. V. Chulhai and J. D. Goodpaster, Improved accuracy and efficiency in quantum embedding through absolute localization, *Journal of Chemical Theory and Computation* **13**, 1503 (2017).
- [33] J. D. Goodpaster, T. A. Barnes, F. R. Manby, and T. F. Miller III, Accurate and systematically improvable density functional theory embedding for correlated wavefunctions, *Journal of chemical physics* **140**, 18A507 (2014).
- [34] D. S. Graham, X. Wen, D. V. Chulhai, and J. D. Goodpaster, Huzinaga projection embedding for efficient and accurate energies of systems with localized spin-densities, *Journal of Chemical Physics* **156**, 054112 (2022).
- [35] D. Claudino and N. J. Mayhall, Simple and efficient truncation of virtual spaces in embedded wave functions via concentric localization, *Journal of Chemical Theory and Computation* **15**, 6085 (2019).
- [36] Q. Sun, T. C. Berkelbach, N. S. Blunt, G. H. Booth, S. Guo, Z. Li, J. Liu, J. McClain, E. R. Sayfutyarova, S. Sharma, S. Wouters, and G. K.-L. Chan, The python-based simulations of chemistry framework (PySCF) (2017), *arXiv:1701.08223* [physics.chem-ph].
- [37] J. R. McClean, K. J. Sung, I. D. Kivlichan, Y. Cao, C. Dai, E. S. Fried, C. Gidney, B. Gimby, P. Gokhale, T. Häner, T. Hardikar, V. Havlíček, O. Higgott, C. Huang, J. Izaac, Z. Jiang, X. Liu, S. McArdle, M. Nee

- ley, T. O'Brien, B. O'Gorman, I. Ozfidan, M. D. Radin, J. Romero, N. Rubin, N. P. D. Sawaya, K. Setia, S. Sim, D. S. Steiger, M. Steudtner, Q. Sun, W. Sun, D. Wang, F. Zhang, and R. Babbush, Openfermion: The electronic structure package for quantum computers, *Quantum Science and Technology* **5** (2017).
- [38] M. Williams and A. Ralli, Nbed, <https://github.com/UCL-CCS/Nbed> (2022).
- [39] P. Jordan and E. Wigner, Über das paulische äquivalenzverbot (1928), *Zeitschrift für Physik* **47**, 631 (1928).
- [40] S. Kim, J. Chen, T. Cheng, A. Gindulyte, J. He, S. He, Q. Li, B. A. Shoemaker, P. A. Thiessen, B. Yu, L. Zaslavsky, J. Zhang, and E. E. Bolton, Pubchem in 2021: new data content and improved web interfaces, *Nucleic Acids Research* **49**, D1388 (2021).
- [41] H. Bergwerf, Molview, <https://molview.org/> (2022), accessed: 2022-02-03.
- [42] A. J. Cohen, P. Mori-Sánchez, and W. Yang, Insights into current limitations of density functional theory, *Science* **321**, 792 (2008).
- [43] A. J. Cohen, P. Mori-Sánchez, and W. Yang, Challenges for density functional theory, *Chemical Reviews* **112**, 289 (2012).
- [44] G. Knizia, Intrinsic atomic orbitals: An unbiased bridge between quantum theory and chemical concepts, *Journal of Chemical Theory and Computation* **9**, 4834 (2013).
- [45] J. Pipek and P. G. Mezey, A fast intrinsic localization procedure applicable for ab initio and semi-empirical linear combination of atomic orbital wave functions, *Journal of Chemical Physics* **90**, 4916 (1989).
- [46] R. S. Mulliken, Electronic population analy-
- sis on lcao-mo molecular wave functions. i, *Journal of Chemical Physics* **23**, 1833 (1955), <https://doi.org/10.1063/1.1740588>.
- [47] J. Foster and S. Boys, Canonical configurational interaction procedure, *Reviews of Modern Physics* **32**, 300 (1960).
- [48] C. Edmiston and K. Ruedenberg, Localized atomic and molecular orbitals, *Reviews of Modern Physics* **35**, 457 (1963).
- [49] I.-M. Høyvik, B. Jansik, and P. Jørgensen, Orbital localization using fourth central moment minimization, *Journal of Chemical Physics* **137**, 224114 (2012).
- [50] M. Svensson, S. Humbel, R. D. Froese, T. Matsubara, S. Sieber, and K. Morokuma, Oniom: a multilayered integrated mo+ mm method for geometry optimizations and single point energy predictions. a test for diels- alder reactions and pt (p (t-bu) 3) 2+ h2 oxidative addition, *The Journal of Physical Chemistry* **100**, 19357 (1996).
- [51] W. M. Kirby and P. J. Love, Classical simulation of non-contextual pauli hamiltonians, *Physical Review A* **102**, 032418 (2020).
- [52] A. Eddins, M. Motta, T. P. Gujarati, S. Bravyi, A. Mezzacapo, C. Hadfield, and S. Sheldon, Doubling the size of quantum simulators by entanglement forging, *PRX Quantum* **3**, 010309 (2022).
- [53] S. Bravyi, J. M. Gambetta, A. Mezzacapo, and K. Temme, Tapering off qubits to simulate fermionic hamiltonians (2017), arXiv:1701.08213 [quant-ph].
- [54] J. P. T. Stenger, D. Gunlycke, and C. S. Hellberg, Expanding variational quantum eigensolvers to larger systems by dividing the calculations between classical and quantum hardware (2021), arXiv:2112.05063 [quant-ph].